REPORT DOCUMENTATION PAGE

Form Approved OMB NO. 0704-0188

1. REPORT DATE (DD-MM-YYYY)	2. REPORT TYPE	3. DATES COVERED (From - To)
31-08-2016	Final Report	23-Apr-2015 - 22-Jan-2016

4. TITLE AND SUBTITLE
Final Report: Designer Solids Nanoantennas and Materials

5a. CONTRACT NUMBER
W911NF-15-1-0138

5b. GRANT NUMBER

5c. PROGRAM ELEMENT NUMBER
611102

6. AUTHORS
Hossein Mosallaei

5d. PROJECT NUMBER

5e. TASK NUMBER

5f. WORK UNIT NUMBER

7. PERFORMING ORGANIZATION NAMES AND ADDRESSES
Northeastern University
360 Huntington Avenue
490 RP
Boston, MA 02115 -5005

8. PERFORMING ORGANIZATION REPORT NUMBER

9. SPONSORING/MONITORING AGENCY NAME(S) AND ADDRESS (ES)
U.S. Army Research Office
P.O. Box 12211
Research Triangle Park, NC 27709-2211

10. SPONSOR/MONITOR'S ACRONYM(S)
ARO

11. SPONSOR/MONITOR'S REPORT NUMBER(S)
66271-EL-II.2

12. DISTRIBUTION AVAILIBILITY STATEMENT
Approved for public release; distribution unlimited.

13. SUPPLEMENTARY NOTES
The views, opinions and/or findings contained in this report are those of the author(s) and should not contrued as an official Department of the Army position, policy or decision, unless so designated by other documentation.

14. ABSTRACT
Integrate plasmonic nanoparticles with designer solids composed of quantum dots (QDs) and molecules to design and engineer multiscale antennas as the building block for materials and devices. We will use a dipole mode approach to create nanoparticles with strong scattering at subwavelength sizes. We will then model clusters of these plasmonic elements integrated with quantum dots. For small size particle only electric dipole mode is required. This modeling will be employed for various nanostructure designs and optimized for desired attributes of energy transmission and absorption

15. SUBJECT TERMS

16. SECURITY CLASSIFICATION OF:			17. LIMITATION OF ABSTRACT	15. NUMBER OF PAGES	19a. NAME OF RESPONSIBLE PERSON
a. REPORT	b. ABSTRACT	c. THIS PAGE			Hossein Mosallaei
UU	UU	UU	UU		19b. TELEPHONE NUMBER 617-373-7354

Report Title

Final Report: Designer Solids Nanoantennas and Materials

ABSTRACT

Integrate plasmonic nanoparticles with designer solids composed of quantum dots (QDs) and molecules to design and engineer multiscale antennas as the building block for materials and devices. We will use a dipole mode approach to create nanoparticles with strong scattering at subwavelength sizes. We will then model clusters of these plasmonic elements integrated with quantum dots. For small size particle only electric dipole mode is required. This modeling will be employed for various nanostructure designs and optimized for desired attributes of energy transmission and absorption.

Enter List of papers submitted or published that acknowledge ARO support from the start of the project to the date of this printing. List the papers, including journal references, in the following categories:

(a) Papers published in peer-reviewed journals (N/A for none)

Received Paper

TOTAL:

Number of Papers published in peer-reviewed journals:

(b) Papers published in non-peer-reviewed journals (N/A for none)

Received Paper

TOTAL:

Number of Papers published in non peer-reviewed journals:

(c) Presentations

B. Barbiellini, L. Hayati, C. Lane, A. Bansil, and H. Mosallaei, “A self-consistent scheme for optical response of large hybrid networks of semiconductor quantum dots and plasmonic metal nanoparticles,” American Physical Society, Baltimore, MD, Mar 14-18, 2016.

Number of Presentations: 0.00

Non Peer-Reviewed Conference Proceeding publications (other than abstracts):

Received Paper

TOTAL:

Number of Non Peer-Reviewed Conference Proceeding publications (other than abstracts):

Peer-Reviewed Conference Proceeding publications (other than abstracts):

Received Paper

TOTAL:

Number of Peer-Reviewed Conference Proceeding publications (other than abstracts):

(d) Manuscripts

Received Paper

TOTAL:

Number of Manuscripts:

Books

Received Book

TOTAL:

Received	Book Chapter

TOTAL:

Patents Submitted

Patents Awarded

Awards

Graduate Students

NAME	PERCENT_SUPPORTED	Discipline
Leili Hayati	1.00	
Christopher Lane	0.10	
FTE Equivalent:	**1.10**	
Total Number:	**2**	

Names of Post Doctorates

NAME	PERCENT_SUPPORTED
Bernardo Barbiellini-Amidel	0.30
FTE Equivalent:	**0.30**
Total Number:	**1**

Names of Faculty Supported

NAME	PERCENT_SUPPORTED	National Academy Member
Hossein Mosallaei	0.50	
Arun Bansil	0.50	
FTE Equivalent:	**1.00**	
Total Number:	**2**	

Names of Under Graduate students supported

NAME	PERCENT_SUPPORTED
FTE Equivalent:	
Total Number:	

Student Metrics

This section only applies to graduating undergraduates supported by this agreement in this reporting period

The number of undergraduates funded by this agreement who graduated during this period: .....

The number of undergraduates funded by this agreement who graduated during this period with a degree in science, mathematics, engineering, or technology fields:.....

The number of undergraduates funded by your agreement who graduated during this period and will continue to pursue a graduate or Ph.D. degree in science, mathematics, engineering, or technology fields:.....

Number of graduating undergraduates who achieved a 3.5 GPA to 4.0 (4.0 max scale):.....

Number of graduating undergraduates funded by a DoD funded Center of Excellence grant for Education, Research and Engineering:.....

The number of undergraduates funded by your agreement who graduated during this period and intend to work for the Department of Defense .....

The number of undergraduates funded by your agreement who graduated during this period and will receive scholarships or fellowships for further studies in science, mathematics, engineering or technology fields: .....

Names of Personnel receiving masters degrees

NAME

Total Number:

Names of personnel receiving PHDs

NAME

Total Number:

Names of other research staff

NAME PERCENT_SUPPORTED

FTE Equivalent:
Total Number:

Sub Contractors (DD882)

Inventions (DD882)

Scientific Progress

We have developed a self-consistent scheme for treating the optical response of large, hybrid networks of semiconducting quantum dots (SQDs) and
plasmonic metallic nanoparticles (MNPs). Our method is efficient and scalable and becomes exact in the limiting case of weakly interacting SQDs. The self-consistent equations obtained for the steady state are analogous to the Heisenberg equations of motion for the density matrix of a SQD placed in an e♂ective electric ♀eld computed within the discrete dipole approximation (DDA). Illustrative applications of the theory to square and honeycomb SQD, MNP and hybrid SDQ/MNP lattices as well as SQD-MNP dimers are presented. Our results demonstrate that hybrid SQD-MNP lattices can provide exible platforms for light manipulation with tunable resonant characteristics.

We have managed a proof of concept model for the system of equations and at the stage to move to next step for highly coupled systems of plasmonic and QDs and more advanced optical systems and multiscale.

Technology Transfer

Designer Solids Nanoantennas and Materials

Hosein Mosallaei

CEM and Physics Lab, Electrical and Computer Engineering Department,

Northeastern University, Boston, MA 02115, USA,

In this STIR project, we establish a powerful framework for exploiting integration of plasmonic nanoparticles with designer solids composed of quantum dots (QDs) and molecules, offering a new paradigm for multiscale energy transfer and material engineering. It will be for the first time that a large array of plasmonic elements will be hybridized with colloidal QDs and modeled to design and engineer multiscale antennas as the building block for materials. We start with a plasmonic particle coupled to a QD to delineate the fundamental underpinnings of the system, and as a pathway for undertaking the modeling of more complex building blocks and large array configurations. We discuss a self-consistent scheme for treating the optical response of large, hybrid networks of semiconducting quantum dots (SQDs) and plasmonic metallic nanoparticles (MNPs). Illustrative applications of the theory to square and honeycomb SQD, MNP and hybrid SDQ/MNP lattices as well as SQD-MNP dimers are presented. Our results demonstrate that hybrid SQD-MNP lattices can provide flexible platforms for light manipulation with tunable resonant characteristics.

1. Introduction

Collective surface charge oscillations (plasmons) on a metal-nanoparticle (MNP) can strongly localize light to subwavelength regions and greatly enhance the field in these regions [1-6]. Gold nanoparticles, for example, are well-known to exhibit plasmonic resonances in the visible [7, 8]. Hybrid systems of MNPs and semiconductor quantum dots (SQDs) [9-15] are attracting special interest because interactions between the excitons of an SQD and the plasmons of an MNP can lead to novel effects and strong modifications of the optical properties of an SQD-MNP network compared to those of the underlying SQD or MNP building blocks; the SQDs play the role of quantum emitters in the network [16, 17], whereas the MNPs act to amplify or dampen the electromagnetic field. The matrix elements of the density operator satisfy the well-known optical Bloch equations [18]. Thus, as shown in [19] the plasmon-excitation interaction leads to the formation of a hybrid excitation with shifted frequency (Lamb shift) and decreased lifetime. The modified decay rate can be also derived from Fermi's golden rule as shown in [7]. Efficient transfer of energy through the network can be achieved by designing a hybrid layer composed of plasmonic elements coupled with SQDs [20] or semiconducting interfaces [21]. The underlying mechanism involves a near-field resonance of electric dipoles, also known as Forster resonance energy transfer (FRET) [22], which can be viewed as a quantum version of the classical resonance phenomenon [23].

The cluster of such systems will be of extreme interests for novel applications, and at the same time challenging to be modeled. To solve such large systems we implement discrete dipole approximation (DDA) which can provide an efficient paradigm for solving the platform. Basically the electromagnetic modes of the plasmonic and quantum dots are derived and the

dipolar modes are considered. The obtained equations differ sharply from the standard linear response treatment in that the SQD density matrix operator can be cast in terms of occupation numbers, which can be computed very efficiently by adapting Self Consistent Field (SCF) iterative scheme. In this way, our method becomes extremely efficient and scalable and enables the treatment of very large hybrid networks. The formulation and obtained results are discussed in the following sections.

2. Method

2.1 Formalism

Our scheme is composed of two main parts, namely, the evaluation of the Heisenberg equations of motion for the density matrix, ϱ, of each SQD in the steady state, and of the effective electric fields calculated within the DDA [24-29]. The density matrix of each SQD is first initialized to the one given by the external electric field E_0. It is next updated by using the local electric field at the SQD. In each of these steps, we solve, in the steady state, given by the master equation

$$\frac{d\rho}{dt} = \frac{i}{h}[\rho, H_E] - \Gamma(\rho) \tag{1}$$

In Eq. 1 $H_E = \hbar\omega_0 \hat{a}^\dagger \hat{a} - \boldsymbol{\mu}\cdot\mathbf{E}\hat{a} - \boldsymbol{\mu}\cdot\mathbf{E}^* \hat{a}^\dagger$ is the SQD Hamiltonian, where $\hat{a}$ and $\hat{a}^\dagger$ are the exciton annihilation and creation operators, ω_0 is the energy gap in the SQD, $\boldsymbol{\mu}$ denotes the dipole matrix element, and $\mathbf{E}$ the electric field. Moreover, Γ is the relaxation matrix where the matrix elements are $\Gamma_{11} = (\varrho_{11} - 1)/\tau_0$, $\Gamma_{22} = \varrho_{22}/\tau_0$, and $\Gamma_{12} = \Gamma^*_{21} = \varrho_{12}\gamma_{21}$.

In order to find the induced polarizations on various elements of the hybrid network within the DDA, we assign polarization $\mathbf{P}_i$ and polarizability $\alpha_i = \varepsilon_0 \chi_i$ [30, 31] to the i^{th} element (plasmonic or semiconducting) of the network. Then $\mathbf{P}_i = \alpha_i \mathbf{E}^i_{loc}$, where $\mathbf{E}^i_{loc}$ is the total (local) electric field on the i^{th} site produced by all other sites and the external electric field. This expression can be expressed into a system of linear equations [32] given by

$$P^i_x = \alpha_i \left[\sum_{i \neq j} \left(G^{ij}_{xx} P^j_x + G^{ij}_{xy} P^j_y \right) + E^0_x \right], \tag{2}$$

$$P^i_y = \alpha_i \left[\sum_{i \neq j} \left(G^{ij}_{yx} P^j_x + G^{ij}_{yy} P^j_y \right) + E^0_y \right],$$

where P_x^i and P_y^i are the *x*- and *y*- components of the polarization at the i^{th} site, and E_x^0 and E_y^0 are the *x*- and *y*- components of the external electric field. G_{ws}^{ij}, with $ws \in \{xx,xy,yx,yy\}$, is a matrix element of the dyadic Green's function $\vec{\vec{\mathbf{G}}}(\mathbf{r},\mathbf{r}')$. The resulting closed form of $\vec{\vec{\mathbf{G}}}(\mathbf{r},\mathbf{r}')$ is given as [33]:

$$\vec{\vec{\mathbf{G}}}(\mathbf{r},\mathbf{r}') = \frac{1}{4\pi\varepsilon_0}\frac{e^{-ik_0R}}{R^3}\left\{\left[(k_0R)^2 - ik_0R - 1\right]\vec{\vec{\mathbf{I}}} - [(k_0R)^2 - 3ik_0R - 3]\mathbf{RR}\right\}, \quad (3)$$

where $\vec{\vec{\mathbf{I}}}$ is the identity dyad, $\mathbf{R}=\mathbf{r}-\mathbf{r}'$, and k_0 is the free space wave vector.

Since our network contains two distinct types of elements (MNP and SQD), we must consider two different forms of linear susceptibility. The classical MNP susceptibility is given by

$$\chi_{MNP}=4\pi\varepsilon_0 a^3\gamma, \quad (4)$$

where *a* is the radius and $\gamma=\frac{\varepsilon_m-\varepsilon_0}{\varepsilon_m+2\varepsilon_0}$ is the effective dielectric constant of the MNP. For the SQD, we use

$$\chi_{SQD} = \frac{1}{3\hbar\varepsilon_{eff}}\frac{2\omega_0\varrho_{11}\mu^2}{(\omega_0-\omega-\gamma_{12})(\omega_0+\omega+\gamma_{12})} \quad (5)$$

where ε_{eff} is given in [19], ϱ_{11} is a matrix element of the density matrix and $1/\gamma_{12}$ is the lifetime of the excited state [34] given by the relaxation matrix.

2.2 Valdidation of the Algorithm

The combined evolution of the density matrix and the induced local polarizations can now be obtained through the preceding set of equations, starting with the initial density matrix $\varrho^{(0)}$ and the resulting susceptibility χ_{SQD} [see Fig. 1]. The linear system in Eq. 2 is solved self-consistently to yield the polarizations on various elements of the network using the local field on each SQD to extract an updated density matrix $\varrho^{(1)}$. The main computational cost as a function of the size of the system is driven by the matrix inversion of the linear system in Eq. 2 which depending on the algorithm the complexity can range from $O(n^2\log n)$ to $O(n^3)$. Here $n=d(N_{MNP}+N_{SQD})$, with *d* being the number of spatial dimensions and N_{MNP} (N_{SQD}) being

the number of MNPs (SQDs) in the system. Self-consistency is reached when $\left|\varrho_{11}^{(n+1)}-\varrho_{11}^{(n)}\right|$ is smaller than a given value: here we used a tolerance of 10^{-5}. In the present calculations, we found that convergence of the density matrix is typically achieved within about 10 iterations, with the number of iterations depending on the external field strength, dipole strength, the distance between the particles and the proximity of the system to the resonance frequency ω_0. However, when μ is large, and the distance between particles is small, we found an increase in the number of iterations to around 30.

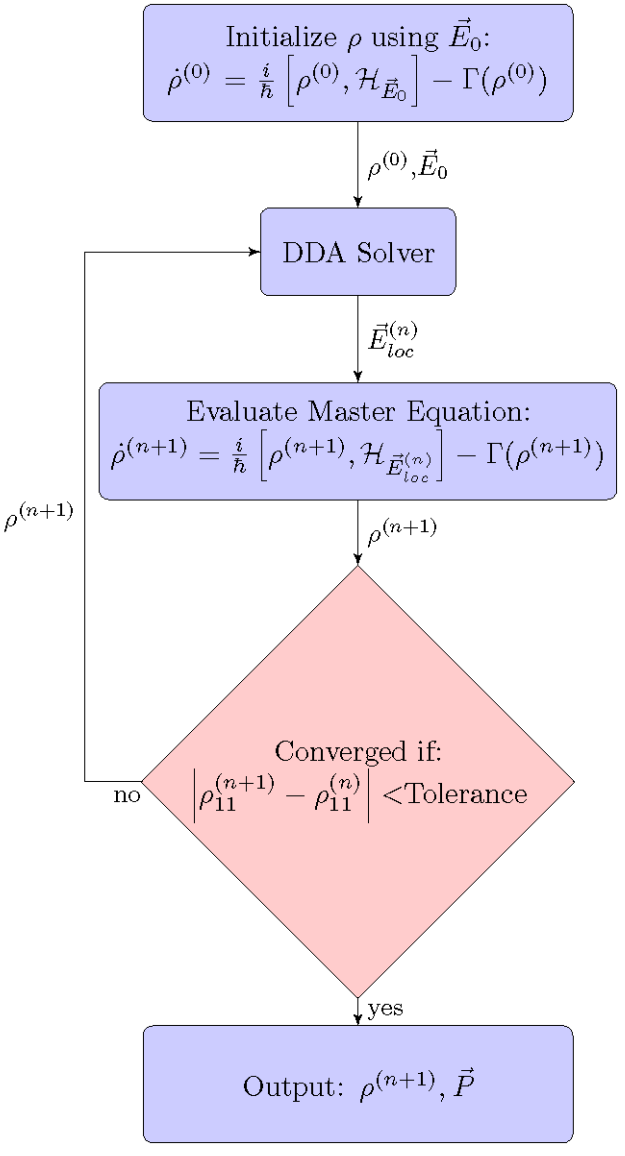

Figure 1: A schematic illustration of our self-consistency loop for treating the network of SQD and MNP elements. Here ϱ^n denotes the density matrix of a SQD in the n^{th} iteration.

The standard route followed in quantum plasmonics involves solving simultaneously the rate equations of the quantum emitters along with the field equations obtained via finite-difference time-domain schemes. The present SCF approach gives the same results in the steady state as the standard approach [19]. However, our scheme avoids the key numerical bottlenecks of the standard approach by invoking the SCF methodology.

3. Results

We first consider the illustrative case of a hybrid dimer composed of a spherical MNP of radius a=7.5 nm and an SQD in the presence of a polarized external field $E_0\cos(\omega t)$, at light intensity of I_0=1 W/cm^2. Plasmonic properties of the MNP are introduced in our calculations by using the dielectric function of Ref. [35]. The energy gap ω_0 of the SQD can be tuned to resonate with the MNP, for example, by modifying the size of the SQD [16]. The dipole moment of the SQD is given by $\mu=e\,r_0$ where we take r_0=0.65 nm, and the relaxation times to be τ_0=0.8 ns for fluorescence and $1/\gamma_{12}$=0.3 ns for the dipole transition. As we mention before the value of γ_{21} and τ_0 are taken from Ref.[19, 36]. The center-to-center distance between the two nano-particles, R, ranges typically between 13 nm to 80 nm. Depending on the angle between the polarization vector and dimer-axis, the two dipoles will interfere either constructively or destructively. In particular, the induced field between the spheres will be enhanced in the longitudinal polarization configuration at frequencies well below the resonance. Figure 2 shows the population of the excited state, ϱ_{22}, for the SQD in the dimer system for different inter-particle distances R when the field is in the longitudinal polarization configuration. The earlier ODE results of Refs. [19, 36] are seen to be almost identical to the present SCF results for R=20 nm, although one can notice small differences at shorter inter-particle distances. The reason is that our self-consistent computation fully captures the feedback of dipole interactions in the system. In fact, in the small R limit, we find that the MNP dominates the response and the SQD becomes irrelevant, while for large R, the behavior of the MNP and SQD contributions is opposite. Our method thus correctly captures the standard ODE cases of dimer as well SQD/MNP/SQD [37] and MNP/SQD/MNP trimers as shown in detail in Fig. 3. Our analysis indicates that for $15\leq R\leq 20$ nm, the hybrid artificial systems (dimer or trimer) behave significantly differently from their constituent elements, and offer unique optical properties at the nanometer scale at their resonant energies.

In particular, when μ is large, our method is able to capture plexitonic effects such as electromagnetically induced transparency (EIT) and modified Fano shapes; it also reproduces well cases studied with the standard ODE approach by Artuso and collaborators [36, 38]. Interestingly, Artuso *et al.* found two distinct solutions to the rate equations [39, 40] due to non-linearity, in the dimer case for a specific set of parameter values (R=13nm,a=7nm,μ=3.5e nm). One of these stable solutions is a smooth and continuous function of ω, while the second solution displays a similarly broad asymmetrical shape away from the resonance with a discontinuous jump. Our method, on the other hand, only yields the first solution. In the strong coupling regime discussed in Ref. [41], the atom-field coupling κ is much larger than the spontaneous decay rate. Such a regime can be accessed by measuring vacuum Rabi oscillations [42].

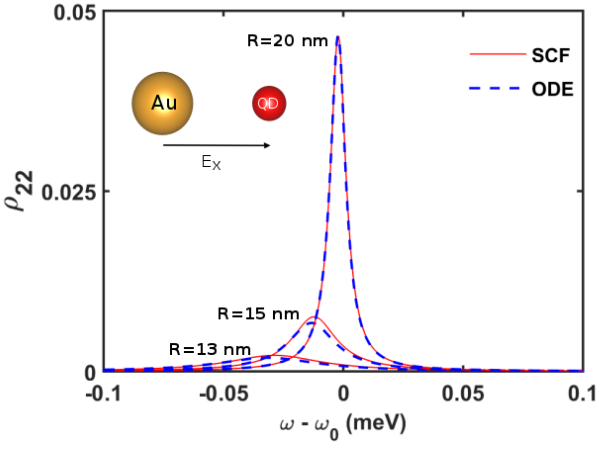

Figure 2: Population of the excited state of a dimer system for different inter-particle distances R. The ODE and SCF results are compared.

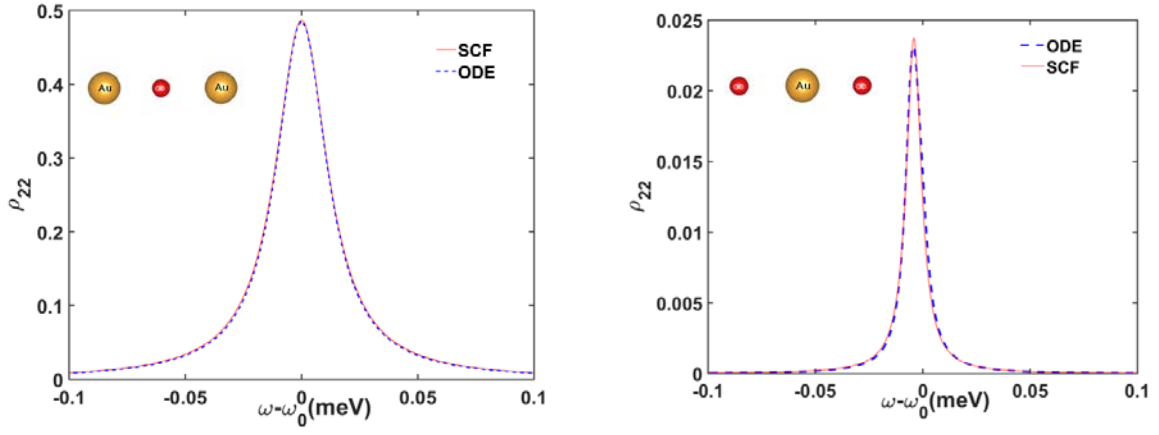

Figure 3: Population of excited states for two different trimers using ODE and SCF methods. Good accord is seen between the results based on the two methods. (a) A MNP-SQD-MNP trimer with: center-to-center

distance R = 20 nm, MNP radius a = 3 nm, dipole moment of QDOT: μ = 0.25 e nm, and light intensity of 10^3 w/cm^2. (b) A SQD-MNP-SQD trimer with: center-to-center distance R=20 nm, MNP radius a = 7.5 nm, dipole moment of QDOTs: μ = 0.5 e nm, and light Intensity of 1 w/cm^2.

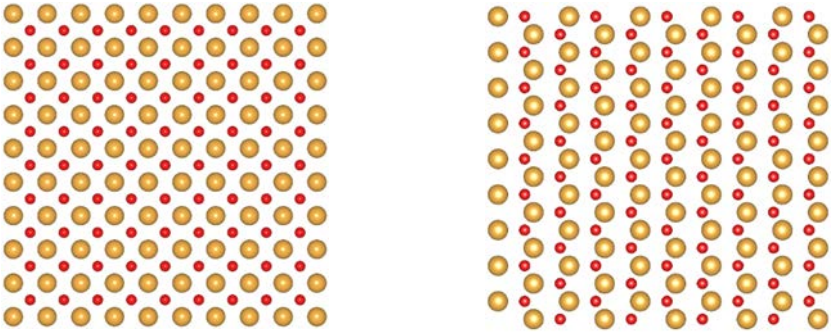

(a) (b)

Figure 4: (a) A 10×10 square MNP lattice with a basis of SQDs; (b) a 10×10 MNP/SQD honeycomb lattice. The gold (red) spheres represent the MNP (SQD).

We turn now to discuss the electromagnetic response of hybrid SQD/MNP lattices by taking advantage of the high computational efficiency of our SCF algorithm. Properties of two specific lattices are considered: a 10×10 square MNP lattice with a basis of SQDs at (0.5,0.5), and a 10×10 MNP/SQD honeycomb lattice, as seen in Fig. 4. Such large systems are intractable within the standard ODE approach [40]. In investigating the SQD/MNP networks, we chose R=20 nm as the distance between the SQD and MNP elements for ease of comparison with the corresponding dimer results. Figure 5 illustrates the resonant behavior of the local electric field E_{loc} as a function of the frequency ω of the external electric field, which is oriented 45° with respect to the x-axis. We observe that on the SQD site of the square lattice there is a strong suppression of the local electric field at the resonance frequency [blue curve in Fig. 5(b)] and that just before the resonance E_{loc} becomes larger than E_0. In the honeycomb lattice also the ratio E_{loc}/E_0 rises just before the resonance but it does not become larger than unity. By comparing various curves in Fig.5, it is clear that there are substantial differences between the behavior of the SQD and MNP lattices, and that the response of the lattices differs sharply from that of the dimer, especially at and near the resonance. Results of Fig. 5 demonstrate that the E_{loc}/E_0 line-shape can be controlled through the choice of the lattice on which elements of the network are arranged, providing flexibility in tuning the plasmonic characteristics of the network. We have also taken advantage of the scalability of our algorithm to find that, near the resonance frequency, the density operator in the infinite lattice limit needs systems as large as 80×80 to converge as illustrated in Fig. 6. Finally, we have simulated effects of disorder by randomly varying the positions of the SQDs and MNPs in the lattice by up to 5% of the inter-particle distance away

from the perfect lattice positions. The resulting uncertainty in the response is shown by the shading around various curves in Fig. 5. It is be seen that the response in all cases considered in Fig. 5 is quite robust against such disorder effects.

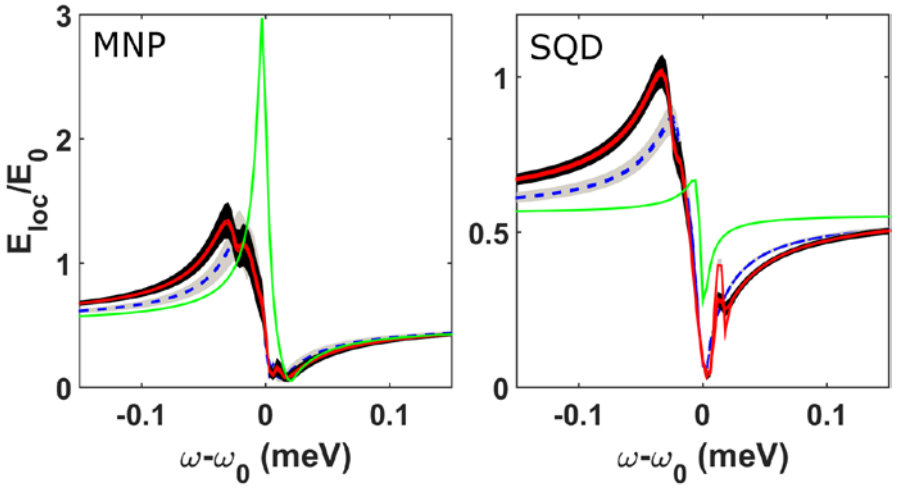

Figure 5: Resonant behavior of the local electric field E_{loc} on MNP (a) and SQD (b) elements of various lattices as a function of the frequency ω: square lattice (blue lines); honeycomb lattice (red lines); and dimer case (green lines). The effect of disorder in the lattice is shown by shading of different colors around various lines. The external field is oriented 45° with respect to the *x*-axis.

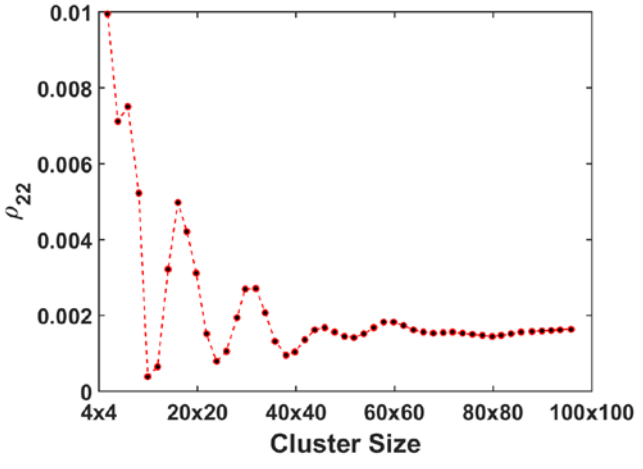

Figure 6: Population of the excited states for the central SQD as a function of lattice (square) size at the frequency ω=ω0. The convergence is reached for systems greater than 80x80.

Figure 7 gives further insight into our results by showing that the hybrid network can be used to shape the electric field in the near-field region by producing a beam with a modulated pattern.

Here, we consider the 10×10 MNP/SQD square network discussed above using the same external field orientation. Figure 7(a) shows the electric field in a plane 12 nm above the planar network for the SQD subnetwork, and is compared with the corresponding results of Fig. 7(b) for the MNP subnetwork [32]. The focal properties of the full hybrid MNP/SQD system (panel (*c*)) are seen to change significantly as demonstrated by the difference, panel (*d*), with respect to the linear superposition of the two pure systems (i.e. MNP and SQD). SQD/MNP arrays could thus provide a flexible basis for designing platforms for nano-antenna light manipulation [43]. Previously, we have noticed that Fig. 5 was little affected by randomness. However, disorder is mainly manifested in the propagation properties. Therefore, quantities shown in Fig. 7, which are relevant to propagation and Green's tensors, are much more sensitive to disorder effects as shown in Fig. 8. Interestingly, disorder in the lattice can also lead to Anderson localization effects, however, here the main reason to introduce small disorder effects is motivated by the study of the stability of our numerical solutions.

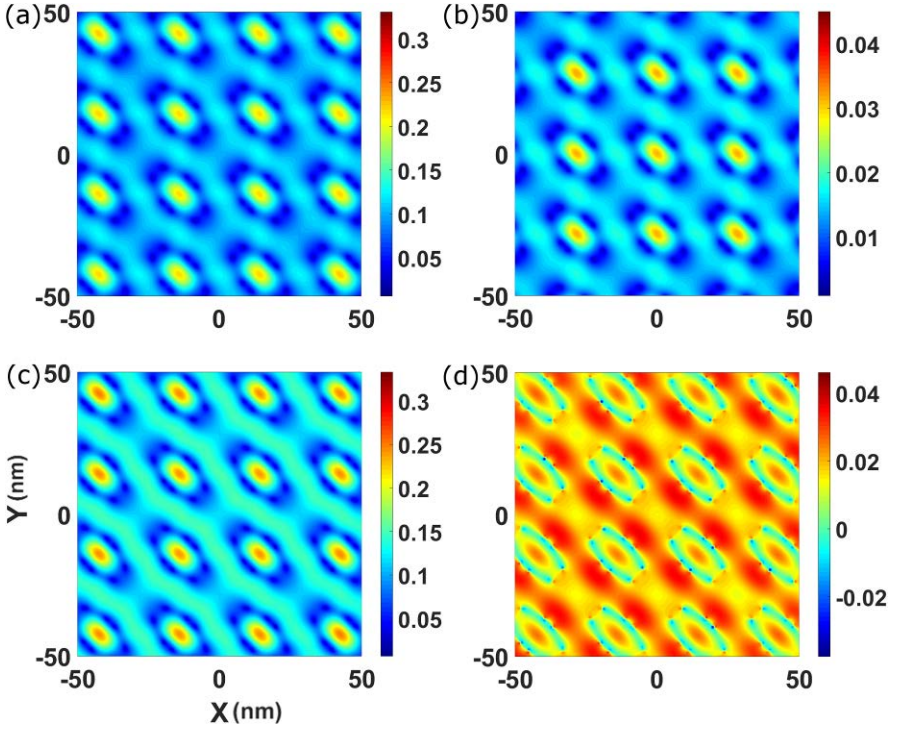

Figure 7: Intensity of the induced electric field (excluding the external field E_0) in a plane 12 nm above the square 10x10 planer network for: (*a*) a pure MNP network; (*b*) a pure SQD network; (*c*) the hybrid MNP/SQD network, and, (*d*) the difference between the hybrid system in (*c*) and the pure MNP system in (*a*). The external field is oriented at 45° with respect to the *x*-axis with ω at resonance. The field intensities are given in units of external field intensity.

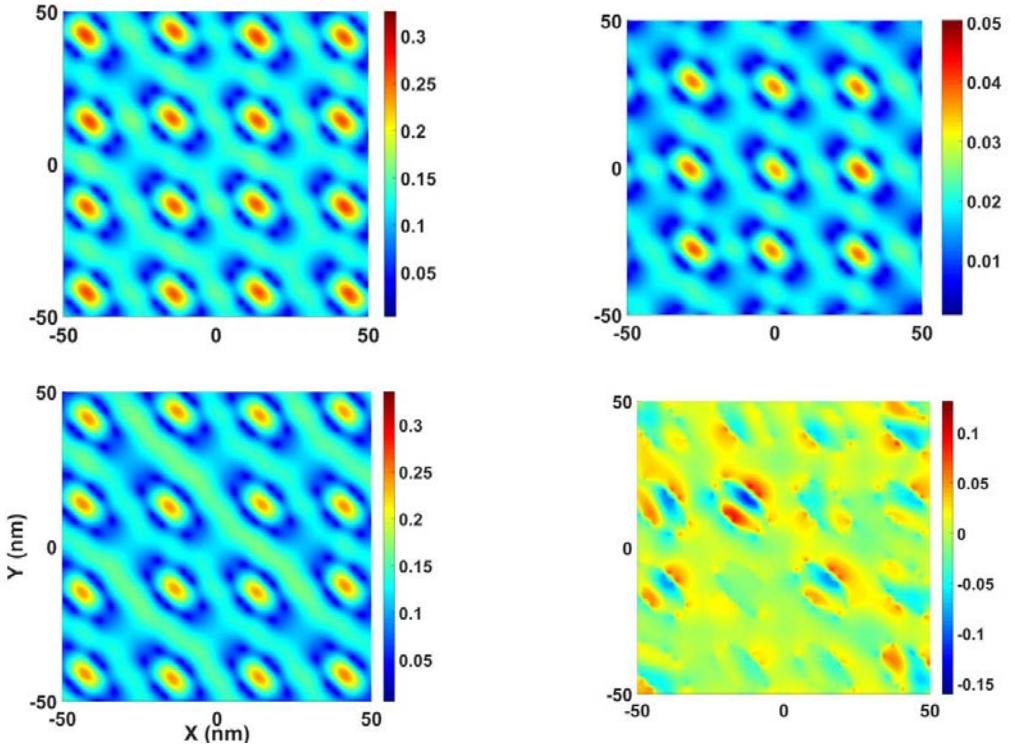

Figure 8: Effects of disorder on the results of Fig. 4 in the main text, where the disorder is simulated by randomly varying the positions of the SQDs and MNPs in the lattice by up to 5% of the inter-particle distance away from the perfect lattice positions.

4. Conclusion

We have developed an efficient SCF method based on the DDA for obtaining the optical response of large networks of plasmonic MNPs and SQDs. Our method is both accurate and scalable, and it can be generalized to treat complex nano-resonators with arbitrary shapes (a next task). The present scheme solves the major computational bottlenecks for the numerical treatment of large hybrid networks of MNPs and SQDs, and significantly advances the field of opto-electronics based on plasmonics. For example, one could determine optimal architectures for absorbing layers in novel quantum dot sensitized solar cells. By combining MNPs with quantum emitters such as the SQD, it will become possible thus to model wireless networks at the nanoscale, and analyze the efficiency of energy transport through such networks.

5. Acknowledgments

This work was supported by the US Army Research Office grant number W911NF-15-1-0138, and benefited from the allocation of computer time at Northeastern University's Advanced Scientific Computation Center (ASCC).

References

[1] H. A. Atwater, Scientific American 296, 56 (2007).
[2] F. G. De Abajo, Reviews of Modern Physics 79, 1267 (2007).
[3] N. Engheta, Science 317, 1698 (2007).
[4] C. Cirac, R. Hill, J. Mock, Y. Urzhumov, A. Fern_andez-Domnguez, S. Maier, J. Pendry, A. Chilkoti, and D. Smith, Science 337, 1072 (2012).
[5] A. Manjavacas and F. G. de Abajo, Nature communications, 5 (2014).
[6] S. Dutta-Gupta and O. J. Martin, JOSA B 32, 194 (2015).
[7] L. Novotny and B. Hecht, Principles of nano-optics (Cambridge university press, 2012).
[8] M. L. Brongersma and P. G. Kik, Surface plasmon nanophotonics (Springer, 2007).
[9] A. O. Govorov, G. W. Bryant, W. Zhang, T. Skeini, J. Lee, N. A. Kotov, J. M. Slocik, and R. R. Naik, Nano letters 6, 984 (2006).
[10] A. G. Curto, G. Volpe, T. H. Taminiau, M. P. Kreuzer, R. Quidant, and N. F. van Hulst, Science 329, 930 (2010).
[11] H. Mertens, J. S. Biteen, H. A. Atwater, and A. Polman, Nano letters 6, 2622 (2006).
[12] Y. Fedutik, V. Temnov, O. Sch□ops, U. Woggon, and M. Artemyev, Physical review letters 99, 136802 (2007).
[13] A. Akimov, A. Mukherjee, C. Yu, D. Chang, A. Zibrov, P. Hemmer, H. Park, and M. Lukin, Nature 450, 402 (2007).
[14] T. Pons, I. L. Medintz, K. E. Sapsford, S. Higashiya, A. F. Grimes, D. S. English, and H. Mattoussi, Nano letters 7, 3157 (2007).
[15] H. Wei and H. Xu, Materials Today 17, 372 (2014).
[16] L. Brus, The Journal of Physical Chemistry 90, 2555 (1986).
[17] C. B. Murray, C. Kagan, and M. Bawendi, Annual Review of Materials Science 30, 545 (2000).
[18] H. Haug and S. W. Koch, Quantum theory of the optical and electronic properties of semiconductors, Vol. 5 (World Scienti_c, 1990).
[19] W. Zhang, A. O. Govorov, and G. W. Bryant, Physical review letters 97, 146804 (2006).
[20] V. Renugopalakrishnan, B. Barbiellini, C. King, M. Molinari, K. Mochalov, A. Sukhanova, I. Nabiev, P. Fojan, H. L. Tuller, M. Chin, et al., The Journal of Physical Chemistry C 118, 16710 (2014).
[21] M. W. Knight, H. Sobhani, P. Nordlander, and N. J. Halas, Science 332, 702 (2011).
[22] C. King, B. Barbiellini, D. Moser, and V. Renugopalakrishnan, Physical Review B 85, 125106 (2012).
[23] D. Ansari-Oghol-Beig, M. Rostami, E. Chernobrovkina, S. K. Saikin, S. Valleau, H. Mosallaei, and A. Aspuru-Guzik, Journal of Applied Physics 114, 164315 (2013).
[24] E. M. Purcell and C. R. Pennypacker, The Astrophysical Journal 186, 705 (1973).
[25] B. T. Draine, The Astrophysical Journal 333, 848 (1988).
[26] B. T. Draine and J. Goodman, The Astrophysical Journal 405, 685 (1993).
[27] B. T. Draine and P. J. Flatau, JOSA A 11, 1491 (1994).
[28] B. T. Draine, Light Scattering by Nonspherical Particles: Theory, Measurements, and Applications 1, 131 (2000).

[29] M. A. Yurkin and A. G. Hoekstra, Journal of Quantitative Spectroscopy and Radiative Transfer 112, 2234 (2011).
[30] A. Ahmadi, S. Ghadarghadr, and H. Mosallaei, Optics express 18, 123 (2010).
[31] A. Alu and N. Engheta, Physical Review B 75, 024304 (2007).
[32] A. Rashidi and H. Mosallaei, Physical Review B 82, 035117 (2010).
[33] H. C. Chen, Theory of electromagnetic waves: a coordinate-free approach (McGraw-Hill Book Company, 1983).
[34] R. W. Boyd, Nonlinear optics (Academic press, 2003).
[35] P. B. Johnson and R.-W. Christy, Physical Review B 6, 4370 (1972).
[36] R. D. Artuso and G. W. Bryant, Nano letters 8, 2106 (2008).
[37] R. D. Artuso and G. W. Bryant, Physical Review B 87, 125423 (2013).
[38] S. Zhang, D. A. Genov, Y. Wang, M. Liu, and X. Zhang, Physical Review Letters 101, 047401 (2008).
[39] R. D. Artuso and G. W. Bryant, Physical Review B 82, 195419 (2010).
[40] R. D. Artuso, Thesis UMD http://hdl.handle.net/1903/13644 (2012).
[41] R. Esteban, J. Aizpurua, and G. W. Bryant, New Journal of Physics 16, 013052 (2014).
[42] P. Vasa, W. Wang, R. Pomraenke, M. Lammers, M. Maiuri, C. Manzoni, G. Cerullo, and C. Lienau, Nature Photonics 7, 128 (2013).
[43] G. M. Akselrod, C. Argyropoulos, T. B. Hoang, C. Ciraci, C. Fang, J. Huang, D. R. Smith, and M. H. Mikkelsen, Nature Photonics 8, 835 (2014).